Int. J. Rock Mech. Min. Sci. & Geomech. Abstr. Vol. 25, No. 3, pp. 171–182, 1988
Printed in Great Britain

0148-9062/88 $3.00 + 0.00
Pergamon Press plc

Poroelastic Response of a Borehole in a Non-hydrostatic Stress Field

E. DETOURNAY*
A. H-D. CHENG†

This paper deals with the solution of the stress, displacement, and pore pressure field induced by the drilling and/or the pressurization of a vertical borehole. The rock, which is permeated by fluid, is assumed to behave as a poroelastic material with compressible constituents, following the Biot theory. The analytical solution is derived in the Laplace transform space, and is transformed to the time domain using an approximate numerical inversion technique. The solution reveals a full range of coupled poroelastic effects which provide potential mechanisms for delayed borehole instability and shear fracture initiation inside the rock.

INTRODUCTION

The mechanical response of fluid-saturated porous rocks is characterized by coupled deformation–diffusion effects. These effects, which are caused by the presence of a pore fluid, can be summarized as follows: (i) excess pore pressures are generated by externally applied loads; (ii) the volumetric deformation of rock is controlled by an "effective" stress; (iii) the gradient of the pore pressure acts like a body force which has to be taken into account in the equilibrium of the effective stress; and (iv) the excess pore pressure is dissipated according to a diffusion law. As a direct consequence of these effects, the volumetric deformation of fluid-saturated rocks exhibits a sensitivity to the rate of isotropic loading, i.e. the rock appears to be stiffer under "fast" than under "slow" loading rate. Under rapid loading, the interstitial fluid has little time to escape (undrained condition) and will resist deformation, thus causing an increase in fluid pressure; under slow compression, excess pore pressure has ample time to dissipate by diffusive transport (drained condition), and therefore does not contribute to the apparent stiffness of the rock. These deformation and diffusion processes are fully coupled; any attempt to model the mechanics of the rock–fluid system should not separate these processes.

The simplest consistent theory which accounts for these coupled hydraulic-mechanical processes is the Biot theory of poroelasticity [1–3]. It differs from the uncoupled theories which have evolved from the earlier work of Terzaghi [4, 5] in the following respects: (i) a pore pressure generation mechanism characterized by the Skempton coefficient [6] is present; (ii) the effective stress governing the deformation of the porous solid is characterized by a coefficient different from that of Terzaghi; and (iii) the pore pressure diffusion law is coupled to the rate of change of the volumetric deformation.

The relevance of poroelasticity to rock mechanics was first discussed by Geertsma [7, 8] thirty years ago, but its significance in various applications has not yet been fully recognized. The Biot theory is particularly important because it predicts effects which are not revealed by the uncoupled theories. The Mandel–Cryer effect [9, 10] and the Noordbergum effect during pumping of an elastic aquifer [11] are classic examples in soil mechanics of the coupling between the diffusion and deformation processes. Demonstration of poroelastic effects in rock mechanics and geophysics have also been made recently. Among other evidences, we would like to cite the dependence of burst pressure on the size of the sample during the pressurization of a hollow rock cylinder [12]; stabilization effects in the propagation of shear and tensile fractures [13–16]; the non-monotonic time variation of the width of a hydraulic fracture [17, 18]; and various effects in earthquakes mechanics such as migration of aftershocks, induced seismicity, and earthquake precursory processes [19].

This paper is concerned with the analysis of the various coupled poroelastic processes triggered by the drilling of a vertical borehole in a saturated formation subjected to a non-hydrostatic *in situ* stress. The analytical solution to this problem is derived in the Laplace transform space, assuming plane strain conditions in the plane perpendicular to the borehole axis, and "instantaneous" drilling; the transformed solution is subsequently inverted numerically to obtain the solution in time. This solution represents a generalization of the results of Carter and Booker [20], which were derived for the limiting case of incompressible fluid and solid constituents (generally known as the soil mechanics case). The results due to various loading conditions are

* Dowell Schlumberger Technology Center, P.O. Box 2710, Tulsa, OK 74101, U.S.A.
† Department of Civil Engineering, University of Delaware, Newark, DE 19716, U.S.A.

examined and analysed, in particular, to provide an explanation of several phenomena observed around excavated and/or pressurized boreholes.

POROELASTICITY

The theory of poroelasticity was first introduced by Biot in 1941 [1]; it has since been re-examined from various angles [2, 3, 11, 12, 21–26]. The approach followed here is that of Rice and Cleary [12] who have provided an elegant reformulation of the Biot theory, in terms of easily identifiable quantities and material constants. This approach has the further advantage that it allows a straightforward interpretation of short- and long-term behaviour of a poroelastic system.

Governing equations

As in the original formulation of Biot [1] (see also Rice and Cleary [12]), the total stress σ_{ij} and the pore pressure p are chosen as the basic dynamic variables (note that tension is here taken positive). The corresponding conjugate kinematic quantities are the solid strain e_{ij}, derivable from an average solid displacement vector u_i, and the variation of fluid content per unit reference volume, ζ. The constitutive equations can be written in terms of these quantities as follows:

$$\sigma_{ij} = 2Ge_{ij} + \frac{2G\nu}{1-2\nu}\delta_{ij}e - \alpha\delta_{ij}p, \tag{1}$$

$$p = -\frac{2GB(1+\nu_u)}{3(1-2\nu_u)}e + \frac{2GB^2(1-2\nu)(1+\nu_u)^2}{9(\nu_u-\nu)(1-2\nu_u)}\zeta, \tag{2}$$

in which δ_{ij} is the Kronecker delta, and the basic material constants are: the shear modulus G, the drained and undrained Poisson's ratios ν and ν_u, and Skempton's pore pressure coefficient B (ratio of the induced pore pressure to the variation of confining pressure under undrained conditions [6]). The parameter α is Biot's coefficient of effective stress which can be defined as

$$\alpha = \frac{3(\nu_u-\nu)}{B(1-2\nu)(1+\nu_u)}. \tag{3}$$

Equation (1) reveals that the "Biot effective stress" $\sigma'_{ij} = \sigma_{ij} + \alpha\delta_{ij}p$, is directly proportional to the solid strain in an identical elasticity relation. Equation (2) indicates that the pore pressure depends linearly on both the deformation of the porous solid and the variation of fluid content.

Besides the constitutive equations (1) and (2), a complete description of the governing equations for poroelasticity consists also of

the equilibrium equations

$$\sigma_{ij,j} = 0, \tag{4}$$

Darcy's law

$$q_i = -\kappa p_{,i}, \tag{5}$$

and the continuity equation for the fluid phase

$$\frac{\partial\zeta}{\partial t} + q_{i,i} = 0, \tag{6}$$

where q_i is the specific discharge vector, and κ the permeability coefficient, which can be expressed as k/μ, where k is the intrinsic permeability (dimension of length squared) and μ the fluid viscosity. In the above, we have neglected the existence of body forces and fluid sources.

Material constants

A set of five bulk material constants is thus required to provide a full description of an isotropic rock–fluid system from a continuum perspective: two elastic constants G and ν [or equivalently the bulk modulus $K = 2G(1+\nu)/3(1-2\nu)$], the parameter κ which characterizes the diffusive transport property of the system, and two poroelastic coefficients B and ν_u (or the undrained bulk modulus K_u) that account for the coupling between deformation and flow processes. All these constants can be measured experimentally [27–29], but very few measured values have actually been published.

In a different approach, the material constants can be obtained by examining the micro-structure of a porous medium [7, 12, 30, 32, 33]. In fact, the choice of the above bulk material constants does not postulate any particular microscopic structure for the porous matrix besides the constraint that the solid phase is linearly elastic*. The micromechanical approach, however, deals with a set of more basic material parameters such as the bulk modulus of the solid and fluid phase, K_s and K_f, the porosity, ϕ, etc. It allows the determination of the parameters for the continuum description on the basis of the micromechanical constants, thus providing insight as to the admissible range of the bulk parameters. Furthermore the micromechanical approach provides a natural way for generalizing the theory to semi-linear or non-linear materials [32, 34].

It has been argued [6, 12, 27] that the realistic range of variation for B is [0, 1]; for α, [0, 1]†; and for ν_u [ν, 0.5] (or correspondingly for K_u, [K, ∞]). By dealing with the micromechanical parameters, a few limiting cases can be examined. For instance, the upper bounds for B, ν_u, and α are simultaneously reached for cases in which both the fluid and solid constituents are incompressible, i.e. $K_s \to \infty$ and $K_f \to \infty$ (in practice, these upper bounds correspond to cases where K_s and K_f are both much greater than K). This limiting case represents the classical soil mechanics model used for the modelling of clay consolidation [1]. Note that the Terzaghi effective stress $\sigma''_{ij} = \sigma_{ij} + p\delta_{ij}$ is here identical to the Biot effective stress σ'_{ij}. On the other hand, for the consolidation of granular soil at shallow depth, the fluid is much more compressible than the solid grains, especially when the entrapped air in the pores is taken into account. We therefore take $K_s \to \infty$, and K_f must be interpreted in the sense of apparent bulk modulus of the gas–fluid mixture.

* The requirement of microscopic homogeneity in some micromechanics models (e.g. Nur and Byerlee [30]) is not necessary, provided that two, instead of one, bulk moduli are introduced for the "non-fluid infiltrated" phase (solid plus pore space) [12, 31].

† A lower bound $3\phi/(2+\phi)$ for α has been derived by Zimmerman *et al.* [34], which is less conservative than the usually quoted lower bound ϕ.

In this case $B = K_f/(K_f + \phi K)$ and $K_u = K_f/\phi + K$, and $\alpha = 1$. This model is identical to that proposed by Verruijt [11, 35].

In another case, we may consider the fluid to be infinitely compressible (gas), i.e. $K_f = 0$. This corresponds to $B = 0$, $K_u = K$, while α is unaffected. The model becomes mathematically equivalent to the theory of thermal stress (uncoupled thermoelasticity). The pore pressure is governed by a homogeneous diffusion equation and interacts with the solid as a body force through the coefficient α; the solid deformation does not generate any pore pressure and is uncoupled from the pressure equation.

Lastly, consider the case of low porosity, $\phi \approx 0$. We find that $K_u \approx K \approx K_s$, $\alpha \approx (K_s/K_p)\phi \approx 0$, where K_p is the inverse of pore volume compressibility [32]; while B is unaffected. In this case the pore pressure has no effect on the solid deformation process. However, since $B \neq 0$, a pore pressure field is nevertheless generated. It is governed by a diffusion law.

Field equations

The governing equations (1, 2, 4–6) can be combined to yield various field equations for the solution of initial/boundary value problems (see for example the equations proposed by Biot [3], McNamee and Gibson [36], Verruijt [37], Rice and Cleary [12]). For the present purpose, they are presented as a Navier equation with a coupling term and a diffusion equation, in terms of the displacement vector u_i and variation of fluid content ζ:

$$G\nabla^2 u_i + \frac{G}{1-2\nu_u} e_{,i} - \frac{2GB(1+\nu_u)}{3(1-2\nu_u)} \zeta_{,i} = 0, \tag{7}$$

$$\frac{\partial \zeta}{\partial t} - c\nabla^2 \zeta = 0, \tag{8}$$

where

$$c = \frac{2\kappa B^2 G(1-\nu)(1+\nu_u)^2}{9(1-\nu_u)(\nu_u-\nu)}, \tag{9}$$

is a generalized consolidation coefficient [12]. Alternatively, equation (8) can be written in terms of pressure

$$\frac{\partial p}{\partial t} - \frac{2\kappa GB^2(1-2\nu)(1+\nu_u)^2}{9(\nu_u-\nu)(1-2\nu_u)} \nabla^2 p = -\frac{2GB(1+\nu_u)}{3(1-2\nu_u)} \frac{\partial e}{\partial t}. \tag{10}$$

For boundary-value problems characterized by the application of constant boundary conditions, the initial ($t = 0^+$) and final ($t = \infty$) solution are simply obtained by solving an elasticity problem with undrained and drained elastic constants, respectively. Consider first the conditions at $t = 0^+$. Initially upon application of the boundary conditions, fluid has not yet escaped from the pores, i.e. $\zeta = 0$, and equation (7) reduces to the classic Navier equation with undrained Poisson's ratio ν_u. Combination of equations (1) and (2) indicates that the initial excess pore pressure p^{0^+} is given by

$$p^{0^+} = -\frac{B}{3}\sigma_{kk}^{0^+}, \tag{11}$$

where repeated index implies summation. At time $t = \infty$, the excess pore pressure has dissipated, i.e. $p^\infty = 0$. Then according to equation (2),

$$\zeta^\infty = \alpha e^\infty. \tag{12}$$

It can be seen, by substituting the above expression for ζ^∞ into equation (7), that equation (7) now reduces to the classic Navier equation with the drained Poisson's ratio ν.

PROBLEM DESCRIPTION

Let us consider a vertical borehole drilled in a porous rock formation that is characterized by a non-hydrostatic horizontal *in situ* stress field, see Fig. 1:

$$\begin{aligned} \sigma_{xx} &= -(P_0 - S_0), \\ \sigma_{yy} &= -(P_0 + S_0), \\ \sigma_{xy} &= 0, \\ p &= p_0. \end{aligned} \tag{13}$$

In the above P_0 and S_0 are, respectively, the far-field mean stress and stress deviator, p_0 the virgin pore pressure. It is assumed that one of the *in situ* principal stresses is parallel to the borehole axis and that x- and y-axes correspond to the two other principal directions.

This problem can be analysed by assuming plane strain conditions and "instantaneous" drilling of the borehole, provided that the time needed to drill over a distance equal to about 5 times the radius a of the borehole is much smaller than a characteristic time $t_c = a^2/c$. The drilling of the borehole is simulated by removing at time $t = 0$ the stresses that were acting on the borehole boundary and setting the pore pressure to zero.

To facilitate the physical interpretation of this problem, the loading is decomposed into three fundamental modes: (i) a far-field isotropic stress; (ii) a virgin pore pressure; and (iii) a far-field stress deviator. Note that modes 1 and 2 above are axisymmetric, while mode 3 is asymmetric. Denoting by the superscript (i), the stress *induced* by the loading mode i, the boundary

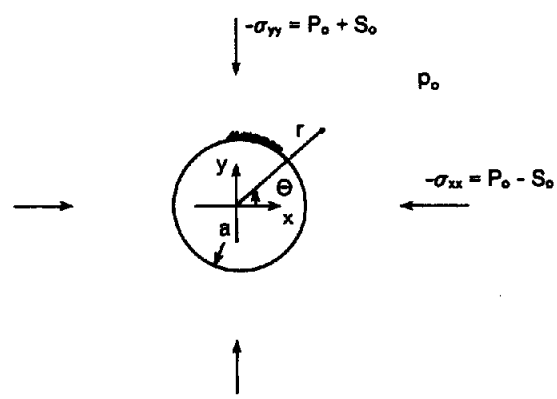

Fig. 1. Problem definition.

conditions at the borehole wall for each of the loading modes can be written as follows.

• mode 1:

$$\sigma_{rr}^{(1)} = P_0$$
$$\sigma_{r\theta}^{(1)} = 0$$
$$p^{(1)} = 0; \tag{14}$$

• mode 2:

$$\sigma_{rr}^{(2)} = 0$$
$$\sigma_{r\theta}^{(2)} = 0$$
$$p^{(2)} = -p_0; \tag{15}$$

• mode 3:

$$\sigma_{rr}^{(3)} = -S_0 \cos 2\theta$$
$$\sigma_{r\theta}^{(3)} = S_0 \sin 2\theta$$
$$p^{(3)} = 0; \tag{16}$$

where r and θ are the polar co-ordinates, defined in Fig. 1. Both the induced stress and pore pressure vanish at infinity. Solutions for the induced stress, pore pressure, and displacement are derived next for each of the fundamental loading modes.

ANALYTICAL SOLUTION

Axisymmetric loading

Calculation of the displacement, stress, and pore pressure induced by the fundamental loading modes 1 and 2 can be carried out in a parallel manner. Indeed, it can be demonstrated [12] that, in the case of a borehole in an infinite domain and under axisymmetric loading, equation (10) can be uncoupled to give a homogeneous diffusion equation

$$\frac{\partial^2 p}{\partial r^2} + \frac{1}{r}\frac{\partial p}{\partial r} = \frac{1}{c}\frac{\partial p}{\partial t}. \tag{17}$$

The pore pressure can therefore be solved independently of the other quantities. After obtaining the general solution of p, the displacement can be calculated by solving equation (7), to give

$$u_r = A\frac{1}{r} + \frac{\eta}{G}\frac{1}{r}\int_a^r rp\, \mathrm{d}r, \tag{18}$$

where η, given by the expression

$$\eta = \frac{3(\nu_u - \nu)}{2B(1-\nu)(1+\nu_u)} = \alpha\frac{1-2\nu}{2(1-\nu)}, \tag{19}$$

is a poroelastic coefficient (the physical range of variation of η is [0–0.5]). It should be noted that in the above the displacement has been required to vanish at infinity.

From equation (18) the polar stress components can be derived easily as follows

$$\sigma_{rr} = -2GA\frac{1}{r^2} - 2\eta\frac{1}{r^2}\int_a^r rp\, \mathrm{d}r,$$
$$\sigma_{\theta\theta} = 2GA\frac{1}{r^2} + 2\eta\frac{1}{r^2}\int_a^r rp\, \mathrm{d}r - 2\eta p,$$
$$\sigma_{r\theta} = 0. \tag{20}$$

The above results are formally identical to those obtained by Carter and Booker [20] for the case of incompressible constituents, except that the material coefficients are now generalized. To get Carter and Booker's solution, we simply use $B = 1.0$ and $\nu_u = 0.5$, which results in the reduced material constant definitions

$$c = \frac{2\kappa G(1-\nu)}{1-2\nu},$$
$$\eta = \frac{1-2\nu}{2(1-\nu)}. \tag{21}$$

The solution of the first two loading modes can now be obtained by introducing the appropriate boundary conditions.

Loading mode 1. For this loading mode, equation (17) yields the trivial solution $p = 0$. In this case, we obtain the classical Lamé solution in elasticity

$$\frac{2Gu_r^{(1)}}{P_0 a} = -\frac{a}{r},$$
$$\frac{\sigma_{rr}^{(1)}}{P_0} = \frac{a^2}{r^2},$$
$$\frac{\sigma_{\theta\theta}^{(1)}}{P_0} = -\frac{a^2}{r^2}. \tag{22}$$

This result could have been also directly derived from the consideration that the rock deformation in this case is entirely associated with the deviatoric strain. As a consequence, there is no mechanism for pore pressure generation, and the displacement and stress field are independent of the bulk modulus of the rock and also of time.

Loading mode 2. In this case, the constant A in equations (18) and (20) vanishes since the total radial stress σ_{rr} at the borehole wall ($r = a$) is equal to zero.

The pore pressure field is solved by taking the Laplace transform of equation (17). Solving this ordinary differential equation with the boundary condition (15), we obtain

$$\frac{s\tilde{p}^{(2)}}{p_0} = -\frac{\mathrm{K}_0(\xi)}{\mathrm{K}_0(\beta)}, \tag{23}$$

where K_0 is the modified Bessel function of second kind of order zero, $\xi = r\sqrt{s/c}$, and $\beta = a\sqrt{s/c}$. It follows from equations (18) and (20) that the Laplace transforms of the displacement, stress and flux fields are

$$\frac{2Gs\tilde{u}_r^{(2)}}{p_0 a} = 2\eta\left[\frac{\mathrm{K}_1(\xi)}{\beta\mathrm{K}_0(\beta)} - \frac{a}{r}\frac{\mathrm{K}_1(\beta)}{\beta\mathrm{K}_0(\beta)}\right], \tag{24}$$

$$\frac{s\tilde{\sigma}_{rr}^{(2)}}{p_0} = -2\eta\left[\frac{a}{r}\frac{\mathrm{K}_1(\xi)}{\beta\mathrm{K}_0(\beta)} - \frac{a^2}{r^2}\frac{\mathrm{K}_1(\beta)}{\beta\mathrm{K}_0(\beta)}\right], \tag{25}$$

$$\frac{s\tilde{\sigma}_{\theta\theta}^{(2)}}{p_0} = 2\eta\left[\frac{a}{r}\frac{\mathrm{K}_1(\xi)}{\beta\mathrm{K}_0(\beta)} - \frac{a^2}{r^2}\frac{\mathrm{K}_1(\beta)}{\beta\mathrm{K}_0(\beta)} + \frac{\mathrm{K}_0(\xi)}{\mathrm{K}_0(\beta)}\right], \tag{26}$$

$$\frac{sa\tilde{q}_r^{(2)}}{p_0\kappa} = -\frac{\beta\mathrm{K}_1(\xi)}{\mathrm{K}_0(\beta)}. \tag{27}$$

Deviatoric loading

For loading mode 3, the solution is also obtained in the Laplace transform domain. Equations (7) and (8) can be Laplace transformed and written in polar coordinates as

$$\frac{1-\nu_u}{1-2\nu_u}\frac{\partial \tilde{e}}{\partial r}-\frac{1}{r}\frac{\partial \tilde{\omega}}{\partial \theta}-\frac{B(1+\nu_u)}{3(1-2\nu_u)}\frac{\partial \tilde{\zeta}}{\partial r}=0, \tag{28}$$

$$\frac{1-\nu_u}{1-2\nu_u}\frac{1}{r}\frac{\partial \tilde{e}}{\partial \theta}+\frac{\partial \tilde{\omega}}{\partial r}-\frac{B(1+\nu_u)}{3(1-2\nu_u)}\frac{1}{r}\frac{\partial \tilde{\zeta}}{\partial \theta}=0, \tag{29}$$

$$\frac{\partial^2 \tilde{\zeta}}{\partial r^2}+\frac{1}{r}\frac{\partial \tilde{\zeta}}{\partial r}+\frac{1}{r^2}\frac{\partial^2 \tilde{\zeta}}{\partial \theta^2}-\frac{s}{c}\tilde{\zeta}=0, \tag{30}$$

where $\tilde{\omega}$ denotes the rotation of the displacement field.

Using symmetry considerations, it can be argued that the dependence of the displacement and stress upon the polar angle θ is of the following form

$$(\tilde{\zeta}^{(3)}, \tilde{e}^{(3)}, \tilde{u}_r^{(3)}, \tilde{\sigma}_{rr}^{(3)}, \tilde{\sigma}_{\theta\theta}^{(3)}, \tilde{p}^{(3)}) = (\tilde{Z}, \tilde{E}, \tilde{U}_r, \tilde{S}_{rr}, \tilde{S}_{\theta\theta}, \tilde{P})\cos 2\theta,$$
$$(\tilde{\omega}^{(3)}, \tilde{u}_\theta^{(3)}, \tilde{\sigma}_{r\theta}^{(3)}) = (\tilde{W}, \tilde{U}_\theta, \tilde{S}_{r\theta})\sin 2\theta, \tag{31}$$

in which $\tilde{Z}$, $\tilde{E}$, $\tilde{W}$, $\tilde{U}_r$, $\tilde{U}_\theta$, $\tilde{S}_{rr}$, $\tilde{S}_{r\theta}$, $\tilde{S}_{\theta\theta}$, and $\tilde{P}$ are functions of r and s only. Substituting the above expressions into equations (28)–(30) produces the set of ordinary differential equations

$$\frac{1-\nu_u}{1-2\nu_u}\frac{d\tilde{E}}{dr}-2\frac{\tilde{W}}{r}-\frac{B(1+\nu_u)}{3(1-2\nu_u)}\frac{d\tilde{Z}}{dr}=0, \tag{32}$$

$$\frac{1-\nu_u}{1-2\nu_u}\frac{\tilde{E}}{r}-\frac{1}{2}\frac{d\tilde{W}}{dr}-\frac{B(1+\nu_u)}{3(1-2\nu_u)}\frac{\tilde{Z}}{r}=0, \tag{33}$$

$$r^2\frac{d^2\tilde{Z}}{dr^2}+r\frac{d\tilde{Z}}{dr}-\left(\frac{s}{c}r^2+4\right)\tilde{Z}=0. \tag{34}$$

Equation (34) can be easily solved for $\tilde{Z}$

$$s\tilde{Z}=C_1' K_2(\xi). \tag{35}$$

After some manipulation, equations (32) and (33) can also be solved to yield

$$s\tilde{W}=C_2'\frac{a^2}{r^2}, \tag{36}$$

$$s\tilde{E}=\frac{B(1+\nu_u)}{3(1-\nu_u)}C_1' K_2(\xi)-\frac{1-2\nu_u}{1-\nu_u}C_2'\frac{a^2}{r^2}. \tag{37}$$

In equations (35)–(37) we have taken into account that $\tilde{Z}$, $\tilde{W}$ and $\tilde{E}$ must vanish at infinity. It is of interest to point out that equation (37) contains a term that does not appear in the solution with incompressible constituents [20].

The displacement components are found by solving equations (36) and (37)

$$\frac{2Gs\tilde{U}_r}{S_0 a}=-\frac{B(1+\nu_u)}{3\beta(1-\nu_u)}C_1\left[K_1(\xi)+\frac{2}{\xi}K_2(\xi)\right]+C_2\frac{a}{r}+C_3\frac{a^3}{r^3}, \tag{38}$$

$$\frac{2Gs\tilde{U}_\theta}{S_0 a}=-\frac{2B(1+\nu_u)}{3\beta^2(1-\nu_u)}C_1\frac{a}{r}K_2(\xi)-\frac{1-2\nu_u}{2(1-\nu_u)}C_2\frac{a}{r}+C_3\frac{a^3}{r^3}. \tag{39}$$

In the above we have redefined the constants C_1' and C_2' into C_1 and C_2. The stress and pore pressure can now be deduced easily from equations (36)–(39):

$$\frac{s\tilde{P}}{S_0}=\frac{B^2(1-\nu)(1+\nu_u)^2}{9(1-\nu_u)(\nu_u-\nu)}C_1K_2(\xi)+\frac{B(1+\nu_u)}{3(1-\nu_u)}C_2\frac{a^2}{r^2}, \tag{40}$$

$$\frac{s\tilde{S}_{rr}}{S_0}=\frac{B(1+\nu_u)}{3(1-\nu_u)}C_1\left[\frac{1}{\xi}K_1(\xi)+\frac{6}{\xi^2}K_2(\xi)\right]-\frac{1}{1-\nu_u}C_2\frac{a^2}{r^2}-3C_3\frac{a^4}{r^4}, \tag{41}$$

$$\frac{s\tilde{S}_{\theta\theta}}{S_0}=-\frac{B(1+\nu_u)}{3(1-\nu_u)}C_1\left[\frac{1}{\xi}K_1(\xi)+\left(1+\frac{6}{\xi^2}\right)K_2(\xi)\right]+3C_3\frac{a^4}{r^4}, \tag{42}$$

$$\frac{s\tilde{S}_{r\theta}}{S_0}=\frac{2B(1+\nu_u)}{3(1-\nu_u)}C_1\left[\frac{1}{\xi}K_1(\xi)+\frac{3}{\xi^2}K_2(\xi)\right]-\frac{1}{2(1-\nu_u)}C_2\frac{a^2}{r^2}-3C_3\frac{a^4}{r^4}. \tag{43}$$

The three constants, C_1, C_2 and C_3, are obtained from the boundary conditions (16). They are

$$C_1=-\frac{12\beta(1-\nu_u)(\nu_u-\nu)}{B(1+\nu_u)(D_2-D_1)},$$
$$C_2=\frac{4(1-\nu_u)D_2}{D_2-D_1},$$
$$C_3=-\frac{\beta(D_2+D_1)+8(\nu_u-\nu)K_2(\beta)}{\beta(D_2-D_1)}, \tag{44}$$

where

$$D_1=2(\nu_u-\nu)K_1(\beta),$$
$$D_2=\beta(1-\nu)K_2(\beta). \tag{45}$$

RESULTS IN TIME DOMAIN

The numerical results in the time domain can be obtained by applying an approximate Laplace inversion to the analytical expressions derived in the preceding section. There exist a great variety of numerical Laplace inversion methods (see the bibliography compiled by Piessens [38]). The numerical results below are carried out using the method of Stehfest [39], which has received high marks [40] for its accuracy, efficiency and stability. The method is based on sampling inversion data according to a delta series. The approximate solution in time is given by the formula

$$f(t)\approx\frac{\ln 2}{t}\sum_{n=1}^{N}C_n\bar{f}\left(n\frac{\ln 2}{t}\right), \tag{46}$$

with the coefficient C_n given by

$$C_n = (-1)^{n+N/2} \sum_{k=(n+1)/2}^{\min(n,N/2)} \frac{k^{N/2}(2k)!}{(N/2-k)!k!(k-1)!(n-k)!(2k-n)!} \quad (47)$$

The number of terms N in the series is even and is typically in the range of 10–20.

We now selectively examine some of the numerical results for mode 2 and mode 3 loading. Note that the background values for the stress and pore pressure have now been added to the induced components (e.g. $p = p_0 + p^{(2)}$ for mode 2), and as a result the superscript (i) has been dropped.

Mode 2

Figure 2 shows isochrones of the normalized tangential stress $\sigma_{\theta\theta}/\eta p_0$ in the vicinity of the borehole (the stress $\sigma_{\theta\theta}/\eta p_0$ is independent of any material properties, and is a function of the two normalized variables $\rho = r/a$ and $t^* = ct/a^2$ only). It can be seen that, except at the borehole wall, the tangential stress history at each point is first compressive (negative), then tensile (positive). The large time asymptotic value $\sigma_{\theta\theta}^{\infty}$, given by the expression

$$\sigma_{\theta\theta}^{\infty} = \eta p_0 \left(1 + \frac{a^2}{r^2}\right), \quad (48)$$

is reached rapidly in the vicinity of the borehole and instantaneously at the borehole wall. (The asymptotic expression (48) can be obtained by setting $p = -p_0$ in equation (20) or inverting equation (26) in the limit of $s \to 0$.) At large distances however, the transition is slow and the asymptotic value is physically impossible to reach, because it corresponds to the total drainage of pore fluid from the domain and the vanishing of the pore pressure everywhere. The small time asymptotic solution can be obtained by an analytical inversion of the expansion of the Laplace transform solution. This result, together with results for other quantities, are presented in the Appendix.

From Fig. 2 we also note that the stress concentration at the borehole wall is tensile in terms of total stress, $\sigma_{\theta\theta} = 2\eta p_0$, but compressive in terms of Terzaghi effective stress, $\sigma_{\theta\theta} + p = (2\eta - 1)p_0$ $(0 \leqslant \eta \leqslant 0.5)$. It is also observed, on the basis of equation (24), that there is no movement of the borehole wall induced by mode 2 loading, although there is a non-zero, inward radial displacement inside the medium. The large time asymptotic value is given by

$$u_r^{\infty} = -\frac{a\eta p_0}{2G}\left(\frac{r}{a} - \frac{a}{r}\right). \quad (49)$$

This value is reached rapidly in the vicinity of the borehole.

The pore pressure and radial flux histories are plotted in Figs 3 and 4 for various distances from the borehole. The initial flat parts of the pressure curves suggest that the drainage area propagate with a relatively steep front. The flux movement is inward and is maximum at the arrival of the front. The maximum rise of the flux diminishes rapidly with distance. At the borehole, the flux is initially infinite and then experiences a continuous decay. For early times, according to the asymptotic solution in the Appendix, the flux varies inversely as the square root of time.

Mode 3

Isochrones of the induced pore pressure variation with distance from the borehole are plotted in Fig. 5, for the parameters $\nu = 0.2$, $\nu_u = 0.4$, $B = 0.8$, and the direction $\theta = 0, \pi$. Upon the instantaneous drilling of the bore-

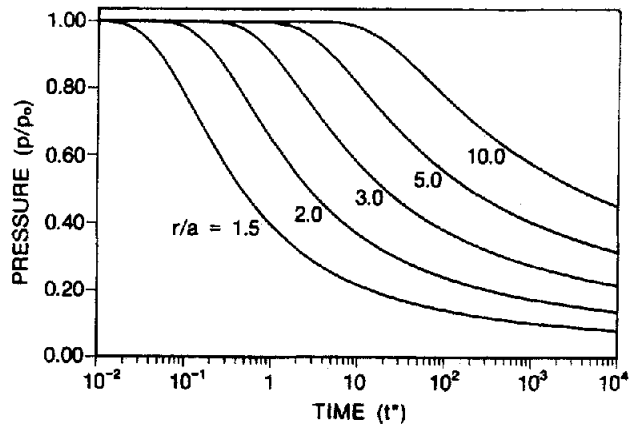

Fig. 3. Pore pressure history at various r/a for mode 2.

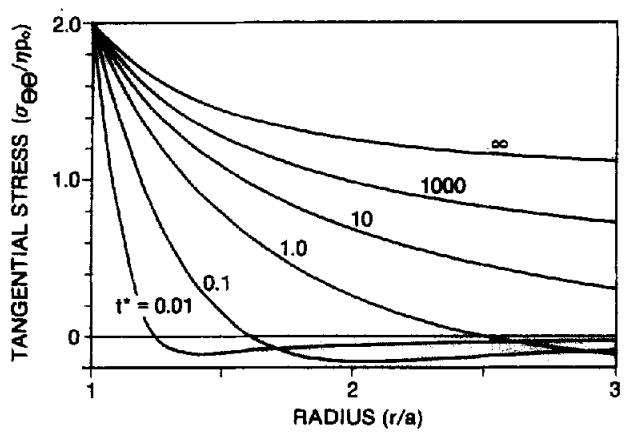

Fig. 2. Isochrones of the tangential stress variation with radius for mode 2.

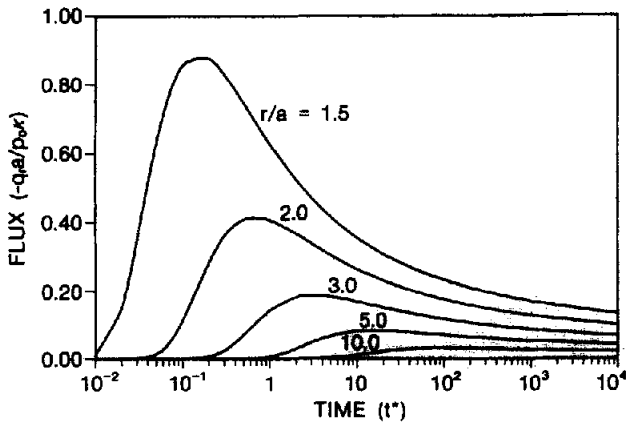

Fig. 4. Radial flux history at various r/a for mode 2.

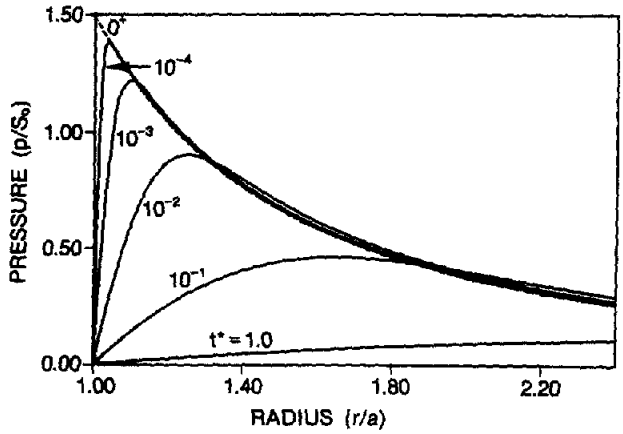

Fig. 5. Isochrones of the pore pressure variation with radius at $\theta = 0$, π for mode 3 ($\nu = 0.2$, $\nu_u = 0.4$, $B = 0.8$).

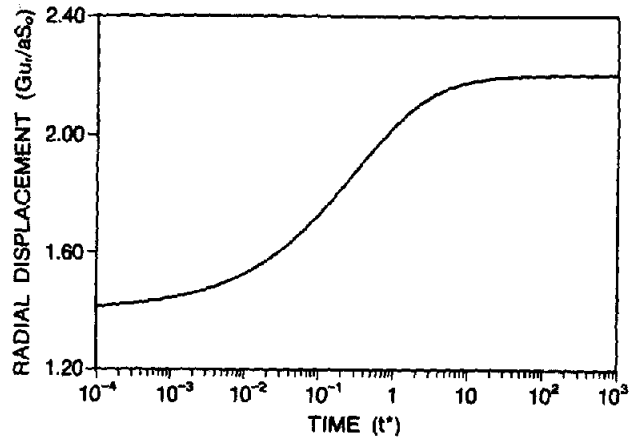

Fig. 7. Radial displacement history at $r/a = 1$, $\theta = 0$, π for mode 3 ($\nu = 0.2$, $\nu_u = 0.4$, $B = 0.8$).

hole, an undrained pore pressure distribution

$$p^{0+} = \frac{4}{3} S_0 B(1 + \nu_u) \frac{a^2}{r^2} \cos 2\theta, \tag{50}$$

is generated, which is plotted as a dashed line in the figure. The enforcement of the boundary condition $p = 0$ is, however, responsible for a steep radial gradient of the pore pressure at early times, which is associated with a rapid drainage of fluid at the wall. (Note that since the pore pressure varies with the polar angle θ, a tangential flow also develops.)

Rapid drainage of the rock near the borehole has a direct impact on the stress concentration. Indeed, at the borehole, the rock is characterized by the drained elastic modulus, while the rock further away is characterized by the stiffer undrained modulus. As a result of this stiffness contrast, the borehole is partially shielded, at early times, from the stress concentration. This effect is well illustrated in Fig. 6 where the isochrones of the tangential stress variation with radial distance have been plotted for the direction $\theta = 0, \pi$. At the instance of drilling, the tangential stress at $r > a$ is given by (see Appendix)

$$\sigma_{\theta\theta}^{0+} = -\left(1 + 3\frac{a^4}{r^4}\right) S_0 \cos 2\theta, \tag{51}$$

which is sketched as a dashed line in the figure. The stress concentration at the borehole wall, $r = a$, however

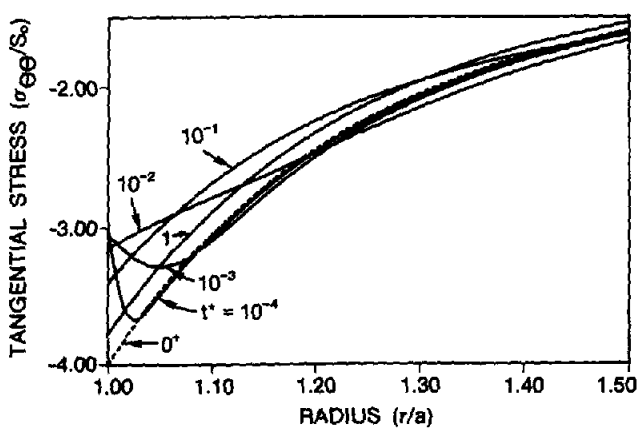

Fig. 6. Isochrones of the tangential stress variation with radius at $\theta = 0$, π for mode 3 ($\nu = 0.2$, $\nu_u = 0.4$, $B = 0.8$).

is instantaneously reduced to

$$\lim_{t \to 0^+} \sigma_{\theta\theta}(a, \theta; t) = -4 \frac{1 - \nu_u}{1 - \nu} S_0 \cos 2\theta. \tag{52}$$

As a result, at very small time ($t^* < 10^{-2}$), the peak of the tangential stress is actually located inside the rock and not at the wall of the borehole, as predicted by the elastic analysis. At greater times, the tangential stress decreases monotonically with distance, and the stress concentration at the wall increases towards the long-term elastic value $4S_0 \cos 2\theta$. It is also interesting to observe that significant deviation of $\sigma_{\theta\theta}$ from the elastic distribution takes place only in a small region near the borehole. It is thus appropriate to describe the poroelastic mechanism as a skin effect. It should be noted that, in contrast to $\sigma_{\theta\theta}$, the radial stress component σ_{rr} experiences little variation.

Finally, the history of the radial displacement at the boundary point $\theta = 0°$ is plotted in Fig. 7. The radial displacement varies from $(3 - 4\nu_u)aS_0/2G$ at small times to $(3 - 4\nu)aS_0/2G$ at large times. Since the radial displacement at the boundary is proportional to $\cos 2\theta$, it can be seen that the existence of a far-field stress deviator produces a time-dependent opening in the direction of the minimum compressive *in situ* stress ("reverse consolidation") and a progressive closure in the perpendicular direction. This phenomenon was first noted by Carter and Booker [20].

APPLICATIONS

As an application of the solution derived above, we examine the role of poroelastic processes on the condition leading to formation breakdown during pressurization of a borehole, and on the stability of a borehole following drilling.

Borehole pressurization

This problem has its root in the hydraulic fracturing technology used by the petroleum industry for stimulating wells. In this technique a section of a borehole is sealed-off, and fluid gradually injected to raise the pressure in that interval. At "breakdown", the fluid

pressure in the borehole is large enough to initiate a fracture in the hydrocarbon formation.

A rigorous study of the breakdown process should be carried out from the perspective of fracture mechanics, by analysing the requirements for the propagation of a pre-existing flaw at the borehole [41–45]. However, it is often simply postulated that breakdown takes place when the Terzaghi effective tensile stress at the borehole wall is equal to the tensile strength, T, of the rock, i.e.

$$\sigma_{\theta\theta} + p = T. \tag{53}$$

The stress concentration induced by pressurization of the borehole ($p = p_w$ and $\sigma_{rr} = -p_w$ at the wall) in the presence of *in situ* stresses can be deduced by superposing the three modes of solutions analysed earlier. Neglecting momentarily the existence of an *in situ* stress deviator S_0, it can be deduced, from equations (22) and (26), that the tangential stress at the borehole wall is

$$\sigma_{\theta\theta} = -2P_0 + 2\eta p_0 + (1 - 2\eta)p_w; \quad r = a. \tag{54}$$

It should be noted that the above equation does not impose any restrictions on how the borehole pressure varies with time. In other words, there is no time lag between the borehole pressure and the resulting stress concentration (this will not be true, however, in the presence of a filter cake). If a far-field stress deviator S_0 exists, the stress concentration due to this loading has to be added to equation (54). This value varies from the expression in equation (52) at small time to the elastic value $4S_0 \cos 2\theta$ at large time.

Taking into account equations (53) and (54), and assuming that the transient deviatoric stress effect has been damped out such that the long-term elastic value prevails, the breakdown pressure is given simply by the expression

$$p_{bl} = \frac{T + 2P_0 - 4S_0 - 2\eta p_0}{2(1 - \eta)}. \tag{55}$$

This expression, first derived by Haimson and Fairhurst [46], represents a lower bound for the breakdown pressure.

Another case of interest is when the fracturing fluid cannot penetrate the rock (sleeve fracturing for example). Through appropriate combination, the predicted breakdown pressure p_{bu}, is

$$p_{bu} = T + 2P_0 - 4S_0 - 2\eta p_0 - (1 - 2\eta)p_i, \tag{56}$$

where p_i is the pore pressure at the borehole wall. Taking a specific example e.g. $P_0/T = 14$, $S_0/T = 2$, $p_0/T = 8$, $\eta = 0.25$. We find that $p_{bl}/T = 11.4$ and $p_{bu}/T = 13.0$ (assuming that $p_i = p_0$). The expression (56) for non-penetrating fluid is seen to yield higher values for the breakdown pressure than equation (55).

Failure initiation around borehole

Previous poroelastic considerations of borehole failure have generally focused on the change of effective stress that accompanies production of the well [47, 48]. Application of the mode 1 and mode 2 solutions discussed above indicates in fact that the effective (Terzaghi) stress concentration at the borehole wall becomes more compressive with reduction of well pressure; with the potential of causing compressive failure at the wall. (It is generally accepted that compressive failure, as well as tensile failure, is controlled by the Terzaghi effective stress [49, 50].) These concepts have been further extended by assuming the rock to behave as a poroelasto-plastic material [51–53].

We are here interested mainly in investigating the role of the poroelastic effects associated with mode 3 loading, in the mechanism of borehole failure following drilling. It will be demonstrated that poroelastic mechanisms can be responsible for a delayed borehole collapse. In addition, the ensuing analysis also suggests that failure can be initiated at a small distance inside the rock, rather than at the borehole wall.

Consider first the borehole stress concentration caused by mode 3 loading. As noted earlier, the short-term solution for the tangential stress at the borehole wall, following drilling, is given by the expression (52). The stress concentration will then increase monotonically with time to the value predicted by the theory of elasticity, see Fig. 8. The magnitude of the variation of the maximum stress concentration is of the order of the *in situ* stress deviator S_0. The characteristic time for this variation is about $t_c \approx a^2/c$ ($t_c^* \approx 1$), but it must be noted that the presence of a filter cake can increase t_c as much as a factor of 10. (An upper bound for this characteristic time can be obtained by solving mode 3 loading with a no-flux boundary condition at the borehole. This solution was obtained by Carter and Booker [20] for the case of incompressible fluid and solid constituents.)

It is worth reiterating that, for constant boundary conditions, mode 3 is the only loading component to introduce time-dependent variation of the stress concentration. Indeed, the borehole response to mode 1 is purely elastic, while the maximum stress concentration induced by mode 2 is reached instantaneously. This time-dependent increase of the stress concentration suggests a possible mechanism for delayed instability of boreholes. In other words, if the compressive strength of the rock is between the small time and large time asymptotic effective stress concentration values, the collapse of the borehole can be delayed for a time as much as $10a^2/c$. It is possible, however, to undertake a more

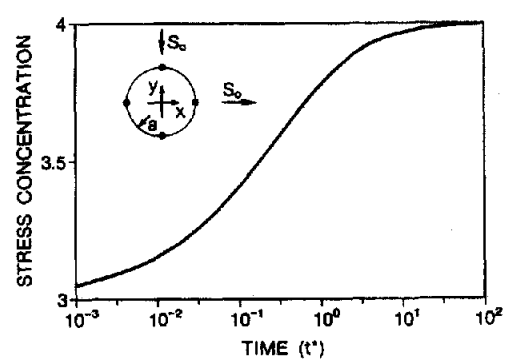

Fig. 8. Stress concentration history at $\theta = 0, \pi$ for mode 3 ($\nu = 0.2$, $\nu_u = 0.4$, $B = 0.8$).

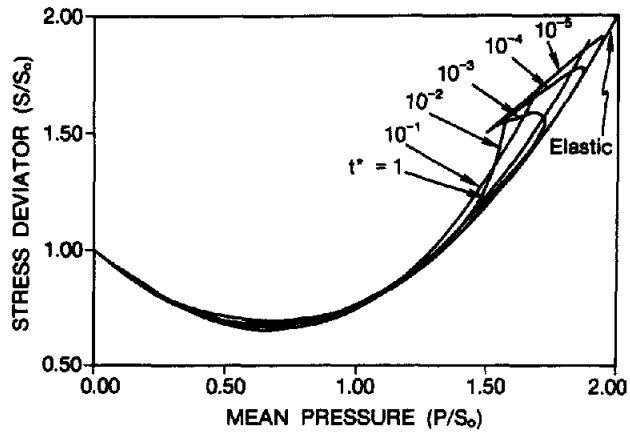

Fig. 9. Isochrones of stress profiles $S - P$ in the radial direction $\theta = 0$, π for mode 3 ($\nu = 0.2$, $\nu_u = 0.4$, $B = 0.8$).

exhaustive analysis of the conditions leading to failure initiation, by considering also the evolution of the state of stress in the vicinity of the borehole in conjunction with a given failure criterion. A condensed way of presenting the stress evolution associated with the failure criterion is to plot, along a given radial direction and at selected times, the maximum planar shear stress S, defined by

$$S = \frac{1}{2}\sqrt{(\sigma_{\theta\theta} - \sigma_{rr})^2 + 4\sigma_{r\theta}^2}, \tag{57}$$

as a function of the mean planar compressive stress P

$$P = -\frac{1}{2}(\sigma_{\theta\theta} + \sigma_{rr}). \tag{58}$$

Figure 9 shows the parametric relationship between S and P along $\theta = 0$ for various times t^*. Figure 10 presents the same plot with the Terzaghi effective mean (compressive) stress $P'' = P - p$ substituted for P. The stress profiles in these figures encompass the range from $r = \infty$ (corresponding to the left ends of the curves where $P = 0$ and $S = S_0$) to the borehole wall (represented by the right ends of the curves which terminate at the intersections with the line $P = S$).

Figure 9 reveals little difference between the curves, except in the region close to the borehole. By contrast,

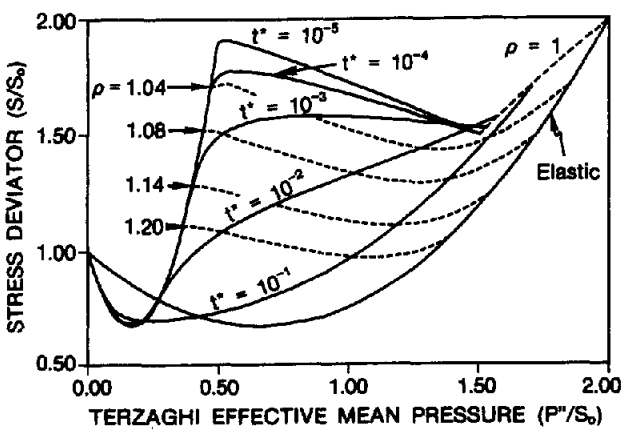

Fig. 10. Isochrones of stress profiles $S - P''$ in the radial direction $\theta = 0$, π and stress history at selected points for mode 3 ($\nu = 0.2$, $\nu_u = 0.4$, $B = 0.8$).

the isochrones of S vs P'' in Fig. 10 reveal a great deal of variation with time. This is a direct consequence of significant pore pressure change over a considerable region induced by mode 3 loading. It is of interest to note that the elastic stress profile given by

$$\frac{S}{S_0} = 1 - \frac{P}{S_0} + \frac{3P^2}{4S_0^2}; \quad 0 \leqslant P \leqslant S, \tag{59}$$

where P should be interpreted as P'', serves as the lower envelope for the family of curves. Another view of the variation is given by displaying the stress history at selected points. These stress histories are shown as dashed lines in the same Fig. 10; they represent the deviatoric vs mean compressive stress relations at selected r for $0 \leqslant t < \infty$.

It is not our intention here to perform an exhaustive study of the conditions of impending failure, but rather to test a conjecture that shear failure can actually initiate inside the rock, rather than at the borehole wall [54]. The following assumptions are made: (i) the failure criterion corresponds to a Mohr–Coulomb envelope, (ii) failure is controlled by the Terzaghi effective stress, and (iii) failure is independent of the out-of-plane normal stress σ_{zz}. Within the constraints of these assumptions, the failure criterion can be expressed as simply as

$$S = \frac{K_p - 1}{K_p + 1}\left(P'' + \frac{q_u}{K_p - 1}\right), \tag{60}$$

where q_u is the uniaxial compressive strength, and K_p the passive coefficient, given in terms of the friction angle ϕ by

$$K_p = \frac{1 + \sin\phi}{1 - \sin\phi}. \tag{61}$$

Considerations of failure require superposition of all the stress modes. Consider the following case characterized by the absence of mode 2: $P_0 = 7$, $S_0 = 1$, $p_0 = p_w = 4$. The corresponding stress profile ($S - P''$) along the x-axis is shown in Fig. 11 for different values of the normalized time t^*. Figure 11 differs from Fig. 10 in that the stresses for mode 1 have now been taken into account.

The straight line in Fig. 11 represents a Mohr–Coulomb criterion criterion characterized by a friction angle $\phi = 30°$ and a uniaxial strength $q_u = 10$. A profile above the line implies failure. As indicated on that figure, these parameters have been chosen in such a way that a state of impending failure exists at the borehole wall (at $\theta = 0$) according to the elastic solution (i.e. the Mohr–Coulomb line intersects with the right end of the elastic stress profile). The figure clearly indicates that failure can indeed initiate at some distance away from the borehole, i.e. not at the borehole wall as is predicted on the basis of the elastic stress distribution. According to the stress history curves (dashed lines), failure occurs at a distance ranging from 5 to 10% of the borehole radius away from the wall. The poroelastic effects associated with mode 3 thus provide a potential mechanism for the formation of borehole breakouts, a pervasive feature of deep wells [55–57].

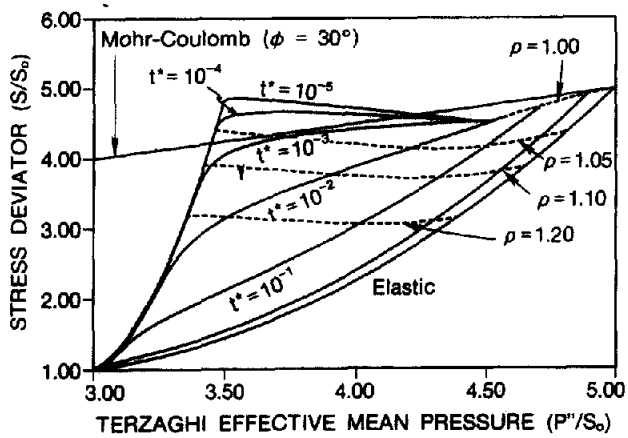

Fig. 11. Determination of the location of shear failure initiation ($\nu = 0.2$, $\nu_u = 0.4$, $B = 0.8$).

The impact of varying the failure parameters q_u and ϕ could be analysed graphically in the diagram of Fig. 11 (note that a change in the compressive strength q_u causes the Mohr–Coulomb envelope to shift up or down, parallel to itself, while variation in the friction angle is reflected by a change in slope of the limiting line). For example, if the friction angle is zero, failure can initiate away from the borehole or at the wall depending on the compressive strength of the material. Note finally that increase in friction angle tends generally to promote initiation of failure inside the rock medium.

CONCLUSIONS

In this paper we have presented an analytical solution to the problem of a vertical borehole drilled in a fluid-saturated poroelastic formation subjected to a non-hydrostatic far-field stress. The solution presented in the paper is a generalization to the poroelastic model of Biot of a solution derived originally by Carter and Booker [20] for the limiting case of incompressible fluid and solid constituents (soil mechanics case).

The poroelastic solution was obtained in closed form in Laplace transform space, and numerically inverted, using the Stehfest algorithm, to retrieve the dependence of the solution upon time. However, asymptotic solutions for small time are derived explicitly as a function of time (see Appendix).

The paper has focused essentially on the poroelastic effects associated with the existence of a far-field stress deviator S_0 (mode 3 loading). We have proven that the undrained elastic solution for the tangential stress and the undrained pore pressure distribution is not the proper short-term solution in the neighbourhood of the borehole. In particular, it was found that the short-term stress concentration associated with mode 3 is $4(1-\nu_u)/(1-\nu)S_0 \cos 2\theta$ and not $4S_0 \cos 2\theta$ as predicted by an elastic analysis.

We have also investigated the conditions of failure initiation based on the poroelastic stress distribution, by assuming the rock to be characterized by a cohesive-frictional strength and failure to be controlled by the Terzaghi effective stress. It was found that shear failure could be initiated *inside* the rock, along a radial direction perpendicular to the *in situ* major compressive stress, rather than at the borehole wall, as is predicted on the basis of an elastic analysis. This finding gives some support to the conjecture that some borehole breakouts actually initiate inside the rock, rather than at the borehole wall.

As a final note, we observe that the poroelastic solution derived in this paper also applies to moderately deviated wells (i.e. for cases where the vertical gradient of the *in situ* stress and pore pressure can be ignored). An anti-plane strain component must however be added to the solution, as the drilling of a borehole inclined to the principal stress directions causes the removal of longitudinal shear stresses along the hole surface. This anti-plane solution causes a local warping of the plane of solution, associated with a shear strain ϵ_{rz}. However, the anti-plane component has no influence either on the volumetric strain and or the mean stress; this component is therefore time-independent and purely elastic.

Acknowledgements—The authors would like to acknowledge with thanks the management of Dowell Schlumberger for allowing publication of this material. They also want to thank Dr J-C. Roegiers for his continuing support of this project.

REFERENCES

1. Biot M. A. General theory of three-dimensional consolidation. *J. Appl. Phys.* **12**, 155–164 (1941).
2. Biot M. A. Theory of elasticity and consolidation for a porous anisotropic solid. *J. Appl. Phys.* **26**(2), 182–185 (1955).
3. Biot M. A. General solutions of the equations of elasticity and consolidation for a porous material. *J. Appl. Mech., Trans. Am. Soc. Mech. Engrs* **78**, 91–96 (1956).
4. Terzaghi K. Die berechnung der durchlassigkeitsziffer des tones aus dem verlauf der hydrodynamischen spannungserscheinungen. *Sber. Akad. Wiss. Wien. Math. Naturwiss. Kl., Abt. IIa* **132**, 105–124 (1923).
5. Rendulic L. Wasserwirt. Techn. **2**, 250 (1935).
6. Skempton A. The pore pressure coefficients A and B. *Geotechnique* **4**, 143–147 (1954).
7. Geertsma J. The effect of fluid pressure decline on volumetric changes of porous rocks. *Petrol. Trans. Am. Inst. Min. Engrs* **210**, 331–340 (1957).
8. Geertsma J. Problems of rock mechanics in petroleum production engineering *Proc. 1st Congr. ISRM*, Lisbon, Vol. 3, pp. 585–594 (1966).
9. Mandel J. Consolidation des sols (étude mathématique). *Geotechnique* **3**, 287–299 (1953).
10. Cryer C. A comparison of the three-dimensional consolidation theories of Biot and Terzaghi. *Q. Jl Mech. Appl. Math.* **16**, 401–412 (1963).
11. Verruijt A. Elastic storage of aquifers. In *Flow Through Porous Media* (Edited by R. J. M. DeWeist). Academic Press, New York (1969).
12. Rice J. R. and Cleary M. P. Some basic stress-diffusion solutions for fluid saturated elastic porous media with compressible constituents. *Rev. Geophys. Space Phys.* **14**, 227–241 (1976).
13. Rice J. R. and Simons D. A. The stabilization of spreading shear faults by coupled deformation diffusion effects in fluid infiltrated porous materials. *J. Geophys. Res.* **81**, 5322–5334 (1976).
14. Simons D. Boundary layer analysis of propagating mode II crack in porous elastic media. *J. Mech. Phys. Solids* **25**, 99–115 (1977).
15. Cleary M. P. Moving singularities in elasto-diffusive solids with applications to fracture propagation. *Int. J. Solids Struct.* **14**, 81–97 (1978).

16. Ruina A. Influence of coupled deformation-diffusion effects on the retardation of hydraulic fracture. *Proc. 19th U.S. Rock Mechanics Symp.*, pp. 274–282 (1978).
17. Detournay E., Roegiers J-C. and Cheng A. H-D. Some new examples of poroelastic effects in rock mechanics. *Rock Mechanics, Proc. 28th U.S. Symp.*, Univ. of Arizona (Edited by I. W. Farmer, J. J. K. Daemen, C. S. Desai, C. E. Glass and S. P. Neuman), pp. 575–584. Balkema, Rotterdam (1987).
18. Cheng A. H-D., Detournay E. and Vandamme L. An integral equation technique for vertical hydraulic fracture in a poroelastic formation. *Proc. 20th Midwestern Mechanics Conf., Development in Mechanics*, Purdue, Vol. 14(b), pp. 591–596 (1987).
19. Rudnicki J. Effects of pore fluid diffusion on deformation and failure of rock. *Mechanics of Geomaterials, Proc. IUTAM William Prager Symp. on Mechanics of Geomaterials: Rocks, Concrete, Soils* (Edited by Z. P. Bazant), Chap. 15, pp. 315–347. Wiley, New York (1985).
20. Carter J. P. and Booker J. R. Elastic consolidation around a deep circular tunnel. *Int. J. Solids Struct.* **18**, 1059–1074 (1982).
21. Crochet M. J. and Naghdi P. M. On constitutive equations for flow of fluid through an elastic solid. *Int. J. Engng Sci.* **4**, 383–401 (1966).
22. Morland L. W. A simple constitutive theory for a fluid-saturated porous solid. *J. Geophys. Res.* **77**, 890–900 (1971).
23. Atkin R. J. and Craine R. E. Continuum theories of mixtures: basic theory and historical developments. *Q. Jl Mech. Appl. Math.* **29**, 209–244 (1976).
24. Bowen R. Theory of mixtures. In *Continuum Physics* (Edited by A. C. Eringen), Vol. 3, pp. 1–127. Academic Press, New York (1976).
25. Carroll M. and Katsube N. The role of Terzaghi effective stress in linearly elastic deformation. *J. Energy Res. Techn.* **105**, 509–511 (1983).
26. Katsube N. and Carroll M. The modified mixture theory for fluid-filled porous materials: theory. *J. Appl. Mech.* **54**, 35–40 (1987).
27. Biot M. A. and Willis D. G. The elastic coefficients of the theory of consolidation. *J. Appl. Mech.* **78**, 91–96 (1956).
28. Fatt I. The Biot–Willis elastic coefficients for a sandstone. *J. Appl. Mech.* **June**, 296–297 (1959).
29. Roeloffs E. Elasticity of saturated porous rocks: laboratory measurements and a crack problem, 157 pp. Ph.D. Thesis, University of Wisconsin, Madison (1982).
30. Nur A. and Byerlee J. D. An exact effective stress stress law for elastic deformation of rock with fluids. *J. Geophys. Res.* **76**, 6414–6419 (1971).
31. Brown R. J. and Korringa J. On the dependence of the elastic properties of a porous rock on the compressibility of the pore fluid. *Geophysics* **40**, 608–616 (1975).
32. Carroll M. Mechanical response of fluid-saturated porous materials. In *Theoretical and Applied Mechanics, 15th Int. Congr. Theoretical & Applied Mechanics*, Toronto (Edited by F. P. J. Rimrott and B. Tabarrok), pp. 251–262 (1980).
33. Katsube N. The constitutive theory for fluid-filled porous materials. *J. Appl. Mech.* **52**, 185–189 (1985).
34. Zimmerman R. W., Somerton W. H. and King M. S. Compressibility of porous rocks. *J. Geophys. Res.* **91**, 12,761–12,777 (1986).
35. Verruijt A. Some remarks on the principle of effective stress. In *Deformation and Failure of Granular Materials, Proc. IUTAM Symp., Delft* (Edited by P. A. Vermeer and H. J. Luger), pp. 167–170. Balkema, Rotterdam (1982).
36. McNamee J. and Gibson R. E. Displacement functions and linear transforms applied to diffusion through porous elastic media. *Q. Jl Mech. Appl. Math.* **13**, 98–111 (1960).
37. Verruijt A. Displacement in the theory of consolidation or in thermoelasticity. *ZAMP* **22**, 891–898 (1971).
38. Piessens R. Bibliography on numerical inversion of the Laplace transform and applications. *J. Comp. Appl. Math.* **1**, 115–126 (1975).
39. Stehfest H. Numerical inversion of Laplace transforms. *Communs. Ass. Comput. Mach.* **13**, 47–49, 624 (1970).
40. Davies B. and Martin B. Numerical inversion of Laplace transform: a survey and comparison of methods. *J. Comp. Phys.* **33**, 1–32 (1979).
41. Abou-Sayed A. S., Brechtel C. E. and Clifton R. J. *In situ* stress determination by hydrofracturing: a fracture mechanics approach. *J. Geophys. Res.* **83**(B6), 2851-2862 (1978).
42. Cleary M. P. Rate and structure sensitivity in hydraulic fracturing of fluid-saturated porous formations. *20th U.S. Rock Mechanics Symp.*, Austin (1979).
43. Alexandre L. G. Note on effects of infiltration on the criterion for breakdown pressure in hydraulic fracturing stress measurements. *Hydraulic Fracturing Stress Measurements* (*Proc. Workshop* December 2–5, 1981), National Academy Press, Washington, DC (1983).
44. Ishijima Y. and Roegiers J.-C. Fracture initiation and breakdown pressure—are they similar? *Proc. 24th Rock Mechanics Symp.*, Austin (1983).
45. Boone T. J., Wawrzynek P. A. and Ingraffea A. R. Simulation of the fracture process in rock with application to hydrofracturing. *Int. J. Rock Mech. Min. Sci. & Geomech. Abstr.* **23**(3), 255–265 (1986).
46. Haimson B. and Fairhurst C. Initiation and extension of hydraulic fractures in rocks. *Soc. Petrol Engrs J.* **September**, 310–318 (1967).
47. Cheatham J. B. Wellbore stability, *J. Petrol. Technol.* **June**, 889–896 (1984).
48. Geertsma J. Some rock-mechanical aspects of oil and gas well completions. *Soc. Petrol Engrs J.* **December**, 848–856 (1985).
49. Rice J. Pore pressure effects in inelastic constitutive formations for fissured rock masses. In *Advances in Civil Engineering Through Engineering Mechanics*, pp. 360–363. ASCE, New York (1977).
50. Cornet F. and Fairhurst C. Influence of pore pressure on the deformation behavior of saturated rocks. In *Proc. 3rd Congr. ISRM*, Denver. National Academy of Sciences, Washington, DC (1974).
51. Bratli R. K. and Risnes R. Stability and failure of sand arches. *Soc. Petrol Engrs J.* **April**, 236–248 (1981).
52. Risnes R., Hosrud P. and Bratli R. K. Sand stresses around a wellbore. *Soc. Petrol Engrs J.* **December**, 883–899 (1982).
53. Bratli R. K., Hosrud P. and Risnes R. Rock mechanics applied to a region near the well bore. *Proc. 5th Congr. ISRM*, Melbourne (1983).
54. Guenot A. Personal communication (1987).
55. Gough D. I. and Bell J. S. Stress orientations from borehole wall fractures with examples from Colorado, east Texas, and northern Canada. *Can. J. Earth Sci.* **19**, 1358–1370 (1982).
56. Zoback M. D., Moos D., Mastin L. G. and Anderson R. N. Well bore breakouts and *in situ* stress. *J. Geophys. Res.* **90**, 5523–5530 (1985).
57. Plumb R. A. and Cox J. W. Stress directions in eastern north America determined to 4.5 km from borehole elongation measurements. *J. Geophys. Res.* **92**, 4805–4816 (1987).

APPENDIX

Small time asymptotic solutions

On the basis of the expansion of Laplace transform solution of modes 2 and 3, it is possible to derive the small time asymptotic solution for the region near the borehole.

Mode 2

$$\frac{p}{p_0} = 1 - \sqrt{\frac{a}{r}}\,\mathrm{erfc}\left(\frac{r-a}{\sqrt{4ct}}\right) - \frac{1}{8}\sqrt{\frac{a}{r}}\left(1-\frac{a}{r}\right)\left[\sqrt{\frac{4ct}{a^2\pi}} \times \exp\left(-\frac{(r-a)^2}{4ct}\right) - \left(\frac{r}{a}-1\right)\mathrm{erfc}\left(\frac{r-a}{\sqrt{4ct}}\right)\right]. \tag{A1}$$

$$\frac{\sigma_{\theta\theta}}{p_0} = 2\eta\left\{\left(\frac{a}{r}\right)^{3/2}\left[\sqrt{\frac{4ct}{a^2\pi}}\exp\left(-\frac{(r-a)^2}{4ct}\right) + \mathrm{erfc}\left(\frac{r-a}{\sqrt{4ct}}\right)\right] - \frac{a^2}{r^2}\sqrt{\frac{4ct}{a^2\pi}} + \frac{1}{8}\sqrt{\frac{a}{r}}\left(1-\frac{a}{r}\right)\left[\sqrt{\frac{4ct}{a^2\pi}}\exp\left(-\frac{(r-a)^2}{4ct}\right) - \left(\frac{r}{a}-1\right)\mathrm{erfc}\left(\frac{r-a}{\sqrt{4ct}}\right)\right]\right\}. \tag{A2}$$

$$\frac{\sigma_{rr}}{p_0} = -2\eta\left\{\left(\frac{a}{r}\right)^{3/2}\left[\sqrt{\frac{4ct}{a^2\pi}}\exp\left(-\frac{(r-a)^2}{4ct}\right) - \left(\frac{r}{a}-1\right)\mathrm{erfc}\left(\frac{r-a}{\sqrt{4ct}}\right)\right] - \frac{a^2}{r^2}\sqrt{\frac{4ct}{a^2\pi}}\right\}. \tag{A3}$$

$$\frac{2Gu_r}{ap_0} = 2\eta\left\{\sqrt{\frac{a}{r}}\left[\sqrt{\frac{4ct}{a^2\pi}}\exp\left(-\frac{(r-a)^2}{4ct}\right) - \left(\frac{r}{a}-1\right)\mathrm{erfc}\left(\frac{r-a}{\sqrt{4ct}}\right)\right] + \frac{a}{r}\sqrt{\frac{4ct}{a^2\pi}}\right\}. \tag{A4}$$

$$\frac{aq_r}{p_0\kappa} = -\sqrt{\frac{a}{r}}\left\{\frac{r}{a}\sqrt{\frac{a^2}{\pi ct}}\exp\left(-\frac{(r-a)^2}{4ct}\right)+\frac{1}{4}\operatorname{erfc}\left(\frac{r-a}{\sqrt{4ct}}\right)\right.$$
$$-\frac{7}{32}\frac{a}{r}\left[\sqrt{\frac{4ct}{a^2\pi}}\exp\left(-\frac{(r-a)^2}{4ct}\right)\right.$$
$$\left.\left.-\left(\frac{r}{a}-1\right)\operatorname{erfc}\left(\frac{r-a}{\sqrt{4ct}}\right)\right]\right\}. \tag{A5}$$

This solution indicates that the maximum (tensile) stress concentration $2\eta p_0$ is reached instantaneously at the borehole. Also, the radial flux at the boundary varies as the inverse of $\sqrt{t}$ for small time.

Mode 3

$$\frac{p}{S_0} = \frac{4}{3}B(1+\nu_u)\left[-\sqrt{\frac{a}{r}}\operatorname{erfc}\left(\frac{r-a}{\sqrt{4ct}}\right)+\frac{a^2}{r^2}\right]\cos 2\theta. \tag{A6}$$

$$\frac{\sigma_{rr}}{S_0} = \left[1-4\frac{a^2}{r^2}+3\frac{a^4}{r^4}\right]\cos 2\theta. \tag{A7}$$

$$\frac{\sigma_{\theta\theta}}{S_0} = \left[-1+4\frac{\nu_u-\nu}{1-\nu}\sqrt{\frac{a}{r}}\operatorname{erfc}\left(\frac{r-a}{\sqrt{4ct}}\right)-3\frac{a^4}{r^4}\right]\cos 2\theta. \tag{A8}$$

$$\frac{\sigma_{r\theta}}{S_0} = \left[-1-2\frac{a^2}{r^2}+3\frac{a^4}{r^4}\right]\sin 2\theta. \tag{A9}$$

$$\frac{2Gu_r}{aS_0} = \left[4(1-\nu_u)\frac{a}{r}-\frac{a^3}{r^3}\right]\cos 2\theta. \tag{A10}$$

$$\frac{2Gu_\theta}{aS_0} = \left[-2(1-2\nu_u)\frac{a}{r}-\frac{a^3}{r^3}\right]\sin 2\theta. \tag{A11}$$

$$\frac{aq_r}{S_0\kappa} = \frac{4}{3}B(1+\nu_u)\left[2\frac{a^3}{r^3}-\sqrt{\frac{a}{r}}\sqrt{\frac{a^2}{\pi ct}}\right.$$
$$\left.\times\exp\left(-\frac{(r-a)^2}{4ct}\right)\right]\cos 2\theta. \tag{A12}$$

The previous equations show that the undrained elastic solution is the correct short-term solution for the displacement field and the stress components σ_{rr} and $\sigma_{r\theta}$. The undrained elastic solution is however not the proper short-term solution, in the near bore-hole region, for the tangential stress $\sigma_{\theta\theta}$ and for the pore pressure p.